NASA Technical Memorandum 101292
AIAA-88-2914

Performance of 10-kW Class Xenon Ion Thrusters

Michael J. Patterson and Vincent K. Rawlin
Lewis Research Center
Cleveland, Ohio

(NASA-TM-101292) PERFORMANCE OF 10-kW CLASS XENON ION THRUSTERS (NASA) 30 p CSCL 21C N88-28088

Unclas
G3/20 0158670

Prepared for the
24th Joint Propulsion Conference
cosponsored by the AIAA, ASME, SAE, and ASEE
Boston, Massachusetts, July 11-13, 1988

NASA

PERFORMANCE OF 10-kW CLASS XENON ION THRUSTERS

Michael J. Patterson and Vincent K. Rawlin
National Aeronautics and Space Administration
Lewis Research Center
Cleveland, Ohio 44135

Abstract

This paper presents performance data for laboratory and engineering model 30cm-diameter ion thrusters operated with xenon propellant over a range of input power levels from approximately 2 to 20 kW. Also presented are preliminary performance results obtained from laboratory model 50cm-diameter cusp- and divergent-field ion thrusters operating with both 30cm- and 50cm-diameter ion optics up to 20 kW input power. These data include values of discharge chamber propellant and power efficiencies, as well as values of specific impulse, thruster efficiency, thrust, and power. The operation of the 30cm- and 50cm-diameter ion optics are also discussed.

Introduction

A program was initiated at the National Aeronautics and Space Administration Lewis Research Center (NASA-LeRC) to identify and extend the physical operating limits of 3 kW mercury ion thruster technology to the 10 kW level power range with inert gases. This was motivated by interest in the near term application of ion thrusters for solar electric propulsion missions in Earth-space [refs. 1-3]. These missions would benefit from the reduction in propulsion system complexity afforded through higher power engine operation. The approach in implementing this activity has been to pursue two parallel paths: (1) assess the feasibility of extending the power range of existing 30cm ion thruster technology, and (2) fabricate and test 50cm ion thrusters.

Higher power engine operation can be achieved by an increase in the maximum electric field strength of the ion optics which results in higher ion currents and/or specific impulse, by a change in propellant to a lower atomic weight (with a consequent increase in specific impulse), or by an increase in the effective ion optics area (engine diameter for cylindrical thrusters). Ion thruster operation in the 2 to 25 kW range and up to 200 kW was demonstrated more than twenty years ago by increasing the ion optics diameter to 50- and 150 centimeters respectively [refs. 4,5]. However, in the intervening two decades since these experimental efforts were concluded, significant advances in ion thruster component technology have been made. These advances include the development of high emission current hollow cathodes, broad-beam, high perveance ion optics, and magnetic multipole plasma containment schemes. Thruster operation utilizing these technologies with xenon propellant is presented herein.

Apparatus and Procedure

Thrusters

The performance of several thrusters was documented over a wide range of power levels with xenon propellant, and is presented herein. These thrusters include; (1) a 30cm diameter engineering-model divergent field J-series thruster (Hughes Research Laboratory-built SN-J8), (2) two 30cm diameter laboratory-model ring-cusp thrusters, (3) a 50cm diameter laboratory-model ring-cusp thruster, and (4) a 50cm diameter laboratory-model divergent field thruster. Figures 1a-e and Table I provide information on the designs of these thrusters.

The 30cm diameter, divergent field, J-series thruster, referred to here as '30DIV', is described in reference 6. The 30cm diameter laboratory-model ring-cusp thrusters, '30RC1' and '30RC2', employ magnetic circuits similar to the thrusters developed by Sovey [ref. 7], and by Beattie et al.[ref. 8], respectively. The aspect ratio of the 30RC2 discharge chamber is somewhat different than the 30RC1 thruster due to a shorter chamber length. The design is simplified (in terms of total numbers of magnet rings in the chamber) from 30RC1, and those originally tested and reported in reference 7. The geometry also does not employ an alnico magnet concentric with the cathode assembly, as does 30RC1. This precludes the possibility of irreversible losses with this magnet due to radiative heat transfer from the cathode, as well as design problems associated with cantilevering this mass at the end of the cathode assembly.

Three distinct magnetic field geometries for a 50cm ring-cusp thruster, identified in Table I as 50RC1, 50RC2, and 50RC3, were investigated. The 50RC1 and 50RC2 geometries incorporated magnet rings on the downstream adapter plate used to mate the chamber to 30cm-diameter optics; consequently, neither magnetic circuit could be characterized with 50cm-diameter ion optics. The 50RC2 configuration is comparable to 50RC1 shown in Figure 1d except for the removal of the magnet ring #1 near the cathode assembly. Configuration 50RC3 is comparable to 50RC1 except for the removal of the three magnet rings (#11 - #13) on the adapter plate. The 50RC3 geometry was characterized with both 30cm- and 50cm-diameter ion optics. When operated with 50cm optics, the downstream cathode potential adapter plate was removed. Both the 30cm- and 50cm-diameter ring-cusp thrusters utilize high field strength samarium-cobalt permanent magnets arranged in rings of alternating polarity along the side and back of the anode potential discharge chamber. The magnetic field lines terminate on the magnet surface forming a cusp, hence the term 'ring-cusp'(RC) thruster. The 50cm diameter divergent field thruster, referred to here as '50DIV', is essentially a scaled 30cm J-series thruster. It incorporates a cathode-pole piece assembly from a J-series thruster, but unlike the 30cm thruster, it uses electromagnets to create the diverging field. The principle differences among these thrusters are the configuration and strength of the magnetic field employed to contain the primary electrons.

Ion optics

The grid specifications for the ion extraction assemblies used in testing these thrusters are described in Table II. The optics used for the performance characterization of the 30DIV and 30RC thrusters were NASA-LeRC-fabricated laboratory hardware which are functionally equivalent to standard J-series optics. Temperature measurements of grids documented herein were obtained with the operation of J-series optics.

Several sets of 50cm-diameter ion optics were fabricated using the same hydroforming and chemical-etch techniques used previously in the fabrication of 30cm-diameter optics [ref. 9]. The performance of the 50cm thrusters described herein were obtained from the operation of a single best-perveance 50cm grid set. This grid set, described in Table II, was fabricated from sintered molybdenum. Due to the preliminary nature of these activities, the 50cm grids were not permanently affixed to a mounting ring structure. Consequently, the grid separation was maintained by using a ring of synthetic mica concentric with the grid periphery. The center-to-center cold spacing for this grid set was 0.75 mm. However, irregularities in the thickness of the mica separator, and irregularities in the grids themselves, resulted in large variations in grid-to-grid spacing (from 0.6 to 1.0 mm) over the beam area.

Facilities

The performance characterization of the thrusters were conducted in the 7.6 m × 21.3 m long, and 4.6 m × 19.2 m long vacuum chambers at the NASA-LeRC

Electric Propulsion Laboratory. A description of these facilities can be found in references 10 and 11, along with a description of the power supplies and propellant feed systems employed in these experiments.

Thruster Performance Calculations

The discharge chamber propellant efficiencies quoted were calculated using correction factors to the neutral flow rate to account for gas ingestion, and corrections to the beam current to account for doubly-charged ions. Although the beam charge-state was not documented during these experiments, a beam current correction factor was used based on doubly-charged ion current values, obtained from figure 1 of reference 10 for inert gases.

Corrections and assumptions used in calculations of overall thruster performance included: (1) a total thrust loss factor equal to contributions from doubly-charged ions times a beam divergence factor (divergence factor assumed to be a constant value of 0.98), (2) a neutralizer mass flow rate equal to 0.067 times the beam current (during testing, some thrusters were characterized without the operation of a neutralizer), (3) a neutralizer coupling voltage of 20 V, and (4) a constant fixed power loss of 0.05 kW due to discharge and neutralizer keeper power and accelerator grid dissipated power (some thrusters were characterized without the operation of discharge or neutralizer keepers).

Results and Discussion

The results obtained from the parallel programs with the 30cm- and 50cm-diameter ion thrusters are presented in separate sections. In each section, the performance of the discharge, ion optics, and thrusters are discussed.

Performance of 30cm-Diameter Ion Thrusters

Discharge Chamber

The discharge chamber performance for the 30DIV, and 30RC thrusters are shown in Figures 2 - 5. The plots show the calculated beam ion production cost, in watts per beam ampere, as a function of measured discharge chamber propellant efficiency.

The results of the discharge chamber performance characterization for the 30DIV (J-series) thruster are presented in Figure 2. Thruster input power levels ranged from approximately 2.9 - 20.4 kW. As indicated, the minimum beam ion production cost was approximately 135 W/A at propellant efficiencies of 90 percent. It is noted that the characterization of this thruster was done using a standard J-series cathode, which was designed for a nominal emission current of 12 A. Under most operating conditions, the emission current requirements significantly exceeded this limit, to a maximum value of approximately 64 A. The minimum beam ion production cost values in Figure 2 are comparable to those previously reported for the J-series thruster at lower power levels [ref. 10, 11]. Discharge voltages at high propellant efficiency ranged from 25 to 36 volts.

In a 567 hour wear-test of the J-series thruster at 10 kW conducted by Rawlin [ref. 12], unacceptably high erosion of the upstream side of the baffle in the cathode-pole piece region was measured. One potential solution to this erosion problem is to eliminate this component. A test was conducted to characterize the performance of the thruster discharge chamber with the baffle and support structure removed from the cathode assembly. These results are presented in Figure 3. Thruster input power levels ranged from approximately 3.6 - 11.4 kW. As indicated, minimum discharge losses of approximately 215 W/A were achieved at propellant efficiencies of 90 percent - a significant degradation in performance. Discharge voltages at high propellant efficiency ranged from 25 to 28 volts.

Another potential solution to the baffle erosion problem is to change from the divergent-field to a ring-cusp discharge chamber which does not incorporate a baffle. A ring-cusp thruster (30RC1) was characterized with xenon propellant up to 8.3 kW input power. These results are shown in Figure 4. Discharge losses as low as approximately 115 W/A were achieved at high propellant efficiency and flow rate. Discharge voltages ranged from approximately 29 to 36 volts.

Preliminary tests were conducted on a ring-cusp thruster with a magnetic geometry (30RC2) similar to that reported by Hughes Research Laboratory [ref. 8]. Results obtained for this thruster are presented in Figure 5. For the flow rates indicated, the thruster input power ranged from approximately 3 - 8.7 kW. The beam ion production costs for any flow rate were in excess of 150 W/A for propellant efficiencies greater than 80 percent. Discharge voltages ranged from approximately 24 to 44 volts at high propellant efficiency. The performance of this geometry is significantly lower than that reported in reference 8. The poor performance of this thruster may be associated with the magnetic field in the region of the cathode assembly, and the short chamber length. However, this remains to be confirmed.

Figure 6 shows 'throttling-curves' for these thrusters. These curves provide a direct comparison of the discharge chamber performance of each thruster. The throttling curves in figure 6 define the minimum beam ion production cost over a range of total propellant flow rates at a fixed discharge chamber propellant efficiency of approximately 90 percent for each thruster. The performance of the 30RC1 and

30DIV thrusters were superior, in terms of lower discharge losses, over the range of flow rates investigated.

Ion Optics

The perveance of the 30cm-diameter NASA-LeRC-fabricated ion optics were evaluated on the 30DIV and 30RC2 thrusters. Figure 7 presents a plot of the beam current as a function of the minimum total extraction voltage for the two thrusters. The beam current (J_b, in amperes) can be related to the total extraction voltage (V_t, in volts) by the following equations:

$$
\begin{aligned}
J_b &= 8.01 \times 10^{-6} V_t^{1.78} \quad \pm 25\% \; for\ 30DIV\ thruster && (1)\\
J_b &= 8.77 \times 10^{-12} V_t^{3.55} \quad \pm 25\% for\ 30DIV\ thruster\ minus\ baffle && (2)\\
J_b &= 2.19 \times 10^{-7} V_t^{2.23} \quad \pm 25\% for\ 30RC2\ thruster && (3)
\end{aligned}
$$

The perveance obtained with the 30cm optics on the 30DIV thruster is consistent with that previously reported (for a smaller current and voltage range) [ref. 10] for standard J-series optics on this thruster. As indicated from Figure 7, the perveance degraded significantly (for $V_t \leq 2000$ V) with these optics when the baffle and support structure were removed from the thruster. This degradation was concurrent with the formation of a conical (axially peaked) current density distribution as measured by a beam probe and the reduction in the beam flatness parameter by 50 percent. Substantially lower perveance with the 30RC2 thruster was also observed. These changes in perveance are presumably due to differences in plasma density distribution across the optics, which is influenced by the axial location of the cathode and the strength of the discharge chamber boundary magnetic fields.

The only active component expected to limit thruster performance (maximum input power) as a result of elevated discharge power levels is the ion extraction system [ref. 13]. The 30cm optics were operated at elevated temperatures at thruster input power levels from approximately 2.9 to 20 kW. The discharge power for these input power levels ranged from approximately 250 to 1720 watts. Detailed temperatures of a standard J-series ion extraction system (optics and titanium mounting ring) were documented as a function of discharge power over this range without beam extraction. Temperatures at several locations along the screen and accelerator grids, and mounting structure, were monitored with thermocouples as the discharge power was controlled by varying the cathode emission current and propellant flow rate. Figure 8 shows the maximum extraction system temperature (as measured at the upstream center of the screen grid) as a function of discharge power for the 30DIV thruster and ion optics. The data fit the equation:

$$T_{max} = 300(P_D) + 290 \pm 15\% \; for \; 0.3 < P_D < 1.8 \; kW \qquad (4)$$

where P_D is the discharge power in kilowatts, and T_{max} is the upstream center screen grid temperature in °C. As indicated, the maximum observed temperatures ranged from approximately 380 to 830 °C - a range below the temperatures where a materials problem would be incurred. The lowest temperatures observed on the extraction assembly (T_{min}) were on the base of the titanium mounting ring. These temperatures can be described by:

$$T_{min} = 200(P_D) + 215 \pm 15\% \qquad (5)$$

over the same discharge power range indicated in equation 4.

Figure 9 shows measured temperatures at the center of the screen and accelerator grid, and on the mounting ring base as a function of time from discharge start-up. The discharge power was approximately 1200 W. As indicated, thermal equilibrium was achieved in approximately 40 minutes.

Overall Thruster Performance

Figures 10 and 11 show the demonstrated thruster efficiency versus specific impulse, and thrust versus specific impulse, obtained for the thrusters. Overall thruster performance for the 30DIV and 30RC thrusters are listed in Table III, including the values of the various correction factors.

In Figure 10 (demonstrated thruster efficiency versus specific impulse near 90 percent total propellant efficiency), efficiencies ranged from 65 - 75 percent for approximately 3150 - 4500 seconds I_{sp} for the 30DIV and 30RC1 thrusters. At lower values of specific impulse, the efficiencies of the 30DIV thruster without baffle, and the 30RC2 thruster were on the order of 3 - 7 percent below those of the 30DIV and 30RC1 thrusters. This difference at the low end of the I_{sp} range is due to the significantly higher values of the beam ion production costs, as seen in Figures 3 and 5. The lower region of I_{sp} equates to lower thruster input power. At these lower power levels, the discharge losses associated with the production of beam ions is a larger fraction of the total power into the thruster; consequently, the overall thruster efficiency is more sensitive to discharge chamber performance in the lower I_{sp} range.

Figure 11 shows calculated thrust as a function of specific impulse for the 30DIV thruster. As indicated over the range of approximately 3000 - 4500 seconds I_{sp}, the thrust ranged from approximately 0.10 - 0.67 Newtons.

Thruster Lifetime

Unacceptably high erosion of the upstream baffle in the J-series thruster has been identified during a 10 kW wear-test [ref. 12]. Subsequent erosion studies with this component have indicated erosion rates that are unacceptably high over the entire range of power levels from 2 - 10 kW. This thruster has insufficient life to be a candidate for high total impulse missions with xenon propellant. Operation of this thruster with the removal of this component would eliminate the erosion, but reduces the performance of the discharge chamber and ion optics by a significant degree as previously discussed. Another potential solution to this erosion problem may be to change to the ring-cusp thruster since it does not incorporate a baffle. Wear-tests of this type thruster have been conducted by Hughes Research Laboratory [ref. 14] with xenon propellant. Results from these tests at 1.3 kW indicate no significant erosion of cathode potential surfaces; however, subsequent wear-tests should be conducted with this type thruster at higher power levels.

Performance of 50cm-Diameter Ion Thrusters

Discharge Chamber

Prior to the completion of the fabrication of 50cm ion optics, the 50cm- diameter ring-cusp discharge chamber was characterized with 30cm ion optics. These results are presented in Figure 12. The best performance in terms of low production cost at high propellant efficiency was achieved with 50RC1. The 50RC1 configuration employed 13 double-layer magnetic rings, three of which were located on the downstream cathode potential adapter plate. Minimum discharge losses of approximately 160 W/A at 90 percent propellant efficiency were achieved with this configuration. Discharge voltages at high propellant efficiency ranged from 22 to 27 volts. These values are believed to be substantially below those documented for any previous ion thruster at propellant efficiencies of interest.

For reasons of expediency, the 50cm-diameter ring-cusp thruster did not employ an anode liner to collect the current away from the magnet surface, or any active cooling of the discharge chamber. Consequently, irreversible losses were occasionally experienced for some magnets in the discharge chamber due to ohmic heating. This occurred primarily for magnet ring #1 near the cathode assembly. A test was conducted with the complete removal of magnetic ring #1. This change, designated as configuration 50RC2, resulted in a severe performance degradation as seen in Figure 12. Minimum discharge losses of approximately 430 W/A were observed, with a maximum propellant efficiency achieved of approximately 60 percent. An examination of the axial magnetic field profile near the cathode assembly indicated that the 50RC2 geometry resulted in a peak field strength downstream of the cathode orifice. The magnetic profile for the 50RC1 configuration had a peak field strength at the plane of the cathode orifice. This increase in the magnetic impedance near the cathode assembly resulted in higher discharge voltages (30 - 38 volts) for the 50RC2 geometry, and in higher discharge losses.

Because they incorporated magnet rings on the downstream adapter plate used to mate the chamber to 30cm-diameter optics, neither 50RC1 nor 50RC2 magnetic circuits could be characterized with 50cm-diameter ion optics. A geometry that could be characterized with both size optics is configuration 50RC3. The results obtained for this configuration with 30cm optics are shown in Figure 12. Minimum discharge losses of approximately 320 W/A at 80 percent propellant efficiency were achieved. Discharge voltages ranged from 25 to 33 volts.

Results obtained from the operation of the ring-cusp (50RC3 configuration) thruster and the divergent-field thruster with 50cm-diameter ion optics are shown in Figures 13 and 14 respectively. As indicated in Figure 13, the discharge losses with the 50cm ring-cusp thruster were approximately 125 W/A at 90 percent propellant efficiency with xenon propellant. This discharge chamber performance is comparable to the best obtained with 30cm-diameter xenon ion thrusters. The maximum input power level was approximately 16.3 kW. Discharge voltages ranged from 24 to 32 volts at high propellant efficiency.

The discharge performance of the 50cm-diameter divergent-field thruster with the 50cm-diameter optics are seen in Figure 14. The production costs were sensitive to total propellant flow into the discharge chamber. The minimum discharge losses with xenon propellant were 175 W/A at high flow rates. Thruster input power levels ranged from approximately 3.7 - 19.6 kW. Discharge voltages ranged from 28 to 33 volts at high propellant efficiency.

As indicated in Figures 12 - 15, the discharge chamber performance (in terms of lowest production cost) was significantly better for the 50RC3 geometry with 50cm ion optics than the other thrusters. The production cost was also less sensitive to propellant flow rate and efficiency than was observed in the 50cm divergent-field thruster. However, the discharge 'stability' was very poor. The operating voltage of the discharge was extremely sensitive to small changes in cathode mass flow rate. In order to process more power through a thruster, the discharge power must be increased. This is accomplished primarily through increasing the cathode emission current. To maintain a constant low discharge voltage at successively higher emission currents normally requires a successively higher cathode mass flow rate. The discharge voltage/cathode mass flow rate curve in ring-cusp thrusters is typically much steeper than that for divergent field thrusters. At higher power levels, changes in total discharge chamber flow rate of less than 5 percent can change the discharge voltage by as much as 100 percent.

Ion Optics

The perveance of the 50cm-diameter ion optics were evaluated on both of the 50cm thrusters. Figure 16 presents a plot of the beam current as a function of the minimum total extraction voltage for the two thrusters with xenon propellant. The beam current (J_b, in amperes) can be related to the total extraction voltage (V_t, in volts) by the following equations:

$$J_b = 1.20 \times 10^{-4} V_t^{1.37} \pm 25\% \; for \; 50RC3 \; thruster \qquad (6)$$

$$J_b = 5.65 \times 10^{-5} V_t^{1.55} \pm 25\% \; for \; 50DIV \; thruster \qquad (7)$$

The results obtained with the 50cm optics on the divergent-field thruster were substantially better than those achieved on the 50cm-diameter ring-cusp thruster. The difference in perveance is probably associated with a difference in plasma density across the ion optics. Cusp-field thrusters typically exhibit current density profiles which are more axially-peaked as compared to divergent-field thrusters. This remains to be confirmed, however, as there were no beam diagnostics available during the operation of the 50cm thrusters.

Also shown on Figure 16 are the data obtained from the operation of 30cm-diameter ion optics on the 30DIV thruster. As indicated, the perveance obtained with the 50cm grids on the 50DIV thruster was only slightly better than that obtained with 30cm grids, and significantly worse than the 30cm grids when operated on the 50RC3 thruster. Based on the increased area the 50cm optics should be capable of extracting a beam current 2.9 times that demonstrated with 30cm optics at a fixed total voltage and equivalent effective acceleration distance. Although the center-to-center cold grid-gap of the 50cm grid set (0.75 mm) was larger than the 30cm grids (0.6 mm), an increase in perveance of

$$2.9 \times (\frac{L_{ea-30}}{L_{ea-50}})^2 \sim 2.5 \qquad (8)$$

would still be anticipated when changing from the 30 to 50cm optics. L_{ea-30} and L_{ea-50} are the effective acceleration lengths for the 30- and 50cm-diameter ion optics. These values can be calculated from the equation published by Kaufman [ref. 15], where

$$L_{ea} = \sqrt{(grid\ gap)^2 + (\frac{screen\ grid\ hole\ dia.}{2})^2}\ . \qquad (9)$$

The non-uniform grid spacing is believed to contribute to the poor performance of the 50cm optics. However this would not fully account bfor the low perveance even if the maximum cold grid-gap spacing of 1.0 mm were used in equation 9. Although the 'hot' grid-gap spacing (during beam extraction) was not measured, differential expansion due to thermal loading may have increased the maximum spacing beyond 1.0 mm. In addition, the radial plasma density for the two 50cm thrusters may be less uniform than that of the 30cm thrusters.

Figure 17 shows beam current versus minimum total extraction voltage obtained with the 30cm optics on the 50RC1 and 50RC3 thrusters, compared to that obtained with the 50cm optics on the 50RC3 thruster. As indicated, the performance of the 30cm optics on the 50cm-diameter cusp-field discharge chamber were substantially better than that achieved with the 50cm optics.

Overall Thruster Performance

Figures 18 and 19 show the demonstrated thruster efficiency versus specific impulse, and thrust versus specific impulse, obtained for the two 50cm thrusters with 50cm-diameter optics. Overall thruster performance for each of the thrusters, including the 50RC1 and 50RC3 configurations with 30cm optics, are listed in Table IV.

In Figure 18 (demonstrated thruster efficiency versus specific impulse near 90 percent total propellant efficiency), typical efficiencies ranged from 60 to 75 percent from approximately 3200 to 4750 seconds I_{sp}. These values are comparable to those achieved with the 30cm ion thrusters [Fig. 10]. At the lower values of specific impulse, the efficiencies of the 50DIV thruster were on the order of 2 to 3 percent below the ring-cusp thruster due to the significantly lower discharge chamber efficiency of this thruster.

Figure 19 shows calculated thrust as a function of specific impulse for the two thrusters with 50cm-diameter ion optics. As indicated over the range of approximately 2750 to 4500 seconds I_{sp}, the thrust ranged from approximately 0.10 to 0.60 Newtons. The thrust which has been demonstrated with the 30cm-diameter ion optics on the 30DIV thruster is comparable to that presently demonstrated with either 50cm thruster with the 50cm-diameter ion optics. Also plotted is the thrust range that would be anticipated with 50cm ion optics operating at a perveance level increased by a factor of the beam-area ratio.

Concluding Remarks

The results obtained from performance characterization of several ion thrusters over an extended power range to 20 kW with xenon propellant were presented. Typical discharge chamber performance for the 30DIV (J-series) thruster was 135 - 155 W/A at propellant efficiencies of 90 percent. A substantial performance degradation was observed when this thruster was operated without the baffle and support structure, two components which undergo severe erosion. Discharge losses as low as 115 W/A at 90 percent propellant efficiency were achieved with a 30cm ring-cusp thruster operating at input power levels up to 8.3 kW.

The performance of 30cm NASA-LeRC-fabricated ion optics were also evaluated. The perveance of the optics obtained on the 30DIV thruster was comparable to that previously reported for J-series optics on this thruster over a smaller current and voltage range. The perveance was significantly less with these optics on the 30DIV thruster when the baffle and support structure were removed, and on the 30RC2 thruster. It is believed that this is due to the formation of an axially peaked current density profile with these geometries.

The 30cm ion optics successfully operated at elevated temperatures at thruster input power levels from 2.9 to 20 kW. Temperature measurements were made of the screen and accelerator grids, and the mounting ring of a J-series ion extraction system over a range of discharge power. Maximum temperatures, as measured on the upstream center of the screen grid, varied from 380 to 830 °C over a discharge power range equivalent to these input power levels.

The overall performance of the 30DIV and 30RC thrusters were documented. Typical thruster efficiencies were in the range of 65 to 75 percent at 3150 to 4500 seconds I_{sp}. Calculated values of thrust over this I_{sp} range were approximately 0.10 to 0.67 Newtons.

Preliminary performance data for a 50cm-diameter ring-cusp ion thruster with both 30- and 50cm-diameter ion optics were documented with xenon propellant up to approximately 16 kW input power. Typical discharge chamber performance with 50cm ion optics was 125 W/A at 90 percent propellant efficiency. The discharge voltage was sensitive to small changes in cathode propellant mass flow rate with the 50RC3 magnetic geometry.

The performance obtained with a 50cm-diameter divergent-field was also documented over a range of approximately 4 - 20 kW. Minimum discharge losses of approximately 175 W/A were achieved at high propellant efficiencies and flows with xenon propellant. The beam ion production cost value was more sensitive to propellant flow rate and efficiency than was observed with the 50cm cusp-field thruster.

The performance of the 50cm-diameter ion optics were evaluated on both 50cm thrusters. The demonstrated perveance was comparable or less than that documented for the operation of 30cm ion optics with xenon propellant. It is believed that the relatively poor performance of these optics are due to a large non-uniform grid gap over the optics span.

The overall performance of the 50cm thrusters were comparable to that documented for the 30DIV (J-series) thruster. Typical thruster efficiencies were in the range of 60 to 75 percent at 3250 to 4750 seconds I_{sp}. Calculated values of thrust over this I_{sp} range were approximately 0.10 to 0.60 Newtons.

References

1. Sponable, J.M., and Penn,J.P., "An Electric Orbital Transfer Vehicle for Delivery of NAVSTAR Satellites," AIAA Paper 87-0985, May 1987.

2. Wilbur, P.J., "Electrostatic Thruster Capabilities for Orbit-Raising and Maneuvering Missions," *Orbit Raising and Maneuvering Propulsion: Research Status and Needs,* edited by L.H. Caveny, Progress in Astronautics and Aeronautics, Vol. 89, AIAA, New York, 1984, pp. 327-344.

3. Kaufman, H.R., and Robinson, R.S., "Electric Thruster Performance for Orbit-Raising and Maneuvering," *Orbit Raising and Maneuvering Propulsion: Research Status and Needs,* edited by L.H. Caveny, Progress in Astronautics and Aeronautics, Vol. 89, AIAA, New York, 1984, pp. 303-326.

4. Reader, P.D., "Experimental Performance of a 50 Centimeter Diameter Electron-Bombardment Ion Rocket," AIAA Paper 64-689, August-September 1964.

5. Nakanishi, S., and Pawlik, E.V., "Experimental Investigation of a 1.5-m-Diameter Kaufman Thruster," AIAA Paper 67-725, September 1967.

6. Schnelker, D.E., Collet, C.R., Kami, S., and Poeschel, R.L., "Characteristics of the NASA/Hughes J-Series 30-cm Engineering Model Thruster," AIAA Paper 79-2077, October 1979.

7. Sovey, J.S., "Improved Ion Containment Using a Ring-Cusp Ion Thruster," Journal of Spacecraft and Rockets, **21**, No. 5, September-October 1984, pp. 488 - 495.

8. Beattie, J.R., Matossian, J.N., Poeschel, R.L., Rogers, W.P., and Martinelli, R., "Xenon Ion Propulsion Subsystem," AIAA Paper 85-2012, September 1985.

9. Rawlin, V.K., Banks, B.A., and Byers, D.C., "Design, Fabrication, and Operation of Dished Accelerator Grids on a 30-CM Ion Thruster," AIAA Paper 72-486, April 1972.

10. Rawlin, V.K., "Operation of the J-Series Thruster Using Inert Gases," AIAA Paper 82-1929, November 1982.

11. Patterson, M.J., "Performance Characteristics of Ring-Cusp Thrusters with Xenon Propellant," AIAA Paper 86-1392, June 1986.

12. Rawlin, V.K., "Internal Erosion Rates of a 10 kW Xenon Ion Thruster," AIAA Paper 88-2912, July 1988.

13. Byers, D.C., and Rawlin, V.K., "Electron Bombardment Propulsion System Characteristics for Large Space Systems," AIAA Paper 76-1039, November 1976.

14. Beattie, J.R., Matossian, J.N., and Robson, R.R., "Status of Xenon Ion Propulsion Technology," AIAA Paper 87-1003, May 1987.

15. Kaufman, H.R., "Technology of Electron-Bombardment Ion Thrusters," *Advances in Electronics and Electron Physics*, Vol. 36, Academic Press, Inc., New York 1974, pp. 265-373.

Table I. Thruster Parameters

Thruster	Ion Extraction Diameter, cm	Discharge Chamber Length, cm	Discharge Chamber Diameter, cm	Magnetic Configuration	Number of Magnet Rings	Approximate Magnetic Field Strength	Cathode Type
30DIV, 30 cm J-series	28.7	14.9	29.0	Divergent-field using Alnico-permanent magnets. Field lines terminate on cathode-potential surfaces.	N/A	Maximum 70 G in volume of the discharge.	Standard J-series cathode
30RC1, 30 cm Ring-cusp		26.7	34.3	Ring-cusp field using SmCo permanent magnets. Field lines terminate on anode potential surfaces.	Total of 6 • 2 Double layers on backplate • 3 Double layers on sidewalls • 1 single layer on downstream pole piece	2700-3200 G on magnet surface at cusp.	Laboratory hollow cathode • 6.3 cm × 0.64 cm dia. Ta body tube • 1.6 mm dia. orifice • Alnico magnet
30RC2, 30 cm Ring-cusp		15.2	29.2		Total of 3 • 1 Double layer on backplate • 1 Single layer on sidewall • 1 Single layer on downstream pole piece	2800-3300 G measured on magnet surface at cusp.	Laboratory hollow cathode • 5.7 cm × 0.64 cm dia. Ta body tube • 0.76 mm dia. orifice
50RC1, 30 cm ion optics on 50 cm Ring-cusp Discharge Chamber		27.6	50.8		Total of 13 • 5 Double layers on backplate • 5 Double layers on sidewall • 3 Double layers on cathode potential adaptor plate	3600-4600 G measured on magnet surface at cusp.	Laboratory hollow cathode • 7.0 cm × 0.64 cm dia. Ta body tube with 3.0 cm dia. radiation fin • 2.0 mm dia. orifice
50RC2, 30 cm ion optics on 50 cm Ring-cusp Discharge Chamber					Identical to 50RC1, except for elimination of magnet ring #1 on backplate.		
50RC3, 30 cm ion optics on 50 cm Ring-cusp Discharge Chamber					Identical to 50RC1, except for elimination of magnet rings #11-#13 on adaptor plate.		
50RC3, 50 cm ion optics on 50 cm Ring-cusp Discharge Chamber	49.0				Identical to 50RC3 (10 magnet rings total).		
50DIV, 50 cm ion optics on 50 cm divergent-field Discharge Chamber		14.9	49.8	Divergent-field using electromagnets. Field lines terminate on cathode potential surfaces.	N/A	~ 70 G maximum in volume of discharge	Standard J-series cathode/pole piece assembly

Table II. Grid Specifications

Design Parameters	Ion Extraction Assembly: 30 cm J-series	30 cm Laboratory	50 cm Laboratory
Manufacturer	Hughes Research Laboratory	Lewis Research Center	Lewis Research Center
	Screen Grid		
Thickness, mm	0.38	0.38	0.38
Hole Diameter, mm	1.91	1.91	1.91
Center-to-Center Spacing, mm	2.21	2.21	2.21
Open Area Fraction	0.67	0.67	0.67
	Accelerator Grid		
Thickness, mm	0.38	0.51	0.38
Hole Diameter, mm	1.14	1.27	1.52
Screen-Accelerator Spacing, mm	0.60 + 0.05 − 0.00	0.60 + 0.05 − 0.00	0.75 + 0.25 − 0.15
Dish Depth, cm	2.2	2.5	5.0
Open Area Fraction	0.24	0.30	0.43
Effective Beam Diameter, cm	28.7	28.7	49

Table III. Demonstrated 30cm Thruster Performance

Thruster	Beam Voltage, V_b, V	Beam Current, J_b, A	Discharge Voltage, V_D, V	Beam Ion Production Cost, W/A	Total Propellant Efficiency, η_u	Thrust Correction Factor, α	Thruster Input Power, P, W	Thrust, F, N	Specific Impulse, I_{sp}, sec.	Thrust-to-Power, F/P, mN/kW	Overall Thruster Efficiency, η_t
30DIV, 30 cm J-series	976	2.64	36.3	160	0.885	0.975	3103	0.130	3252	41.9	0.669
	1116	2.71	36.3	155	0.898	0.970	3550	0.142	3509	40.0	0.688
	1316	2.79	36.3	150	0.910	0.962	4196	0.158	3833	37.5	0.706
	1331	4.87	31.1	161	0.908	0.964	7415	0.277	3851	37.4	0.706
	1411	4.92	31.1	159	0.912	0.961	7874	0.287	3970	36.5	0.710
	1511	4.99	31.1	156	0.917	0.957	8471	0.300	4113	35.4	0.715
	1358	7.60	28.2	160	0.863	0.982	11,743	0.445	3764	37.9	0.699
	1508	8.80	27.7	177	0.902	0.968	15,051	0.535	4086	35.5	0.712
	1729	8.88	27.6	169	0.905	0.966	17,074	0.577	4382	33.8	0.726
	1908	8.02	28.2	150	0.893	0.972	16,721	0.551	4571	32.9	0.739
30DIV, baffle and support structure removed	1384	2.48	28.1	351	0.893	0.972	4405	0.145	3894	32.9	0.629
	1647	3.48	25.5	306	0.888	0.974	6910	0.222	4232	32.2	0.668
	1870	5.29	24.8	214	0.886	0.975	11,172	0.360	4505	32.3	0.712
30RC1, 30 cm Ring-cusp	927	2.12	35.5	183	0.925	0.947	2450	0.099	3216	40.4	0.637
	1347	3.13	31.2	138	0.921	0.952	4760	0.177	3882	37.2	0.707
	1622	4.36	34.1	121	0.920	0.953	7728	0.270	4260	35.0	0.731
30RC2, 30 cm Ring-cusp	1220	2.00	39.5	205	0.879	0.977	2948	0.111	3617	37.6	0.667
	1424	2.91	43.5	185	0.871	0.980	4789	0.174	3882	36.3	0.692
	1518	4.22	31.2	180	0.912	0.961	7299	0.256	4118	35.0	0.707
	1706	4.57	25.9	170	0.839	0.986	8715	0.301	4123	34.5	0.698

Table IV. Demonstrated 50cm Thruster Performance

Thruster	Beam Voltage, V_b, V	Beam Current, J_b, A	Discharge Voltage, V_D, V	Beam Ion Production Cost, W/A	Total Propellant Efficiency, η_u	Thrust Correction Factor, α	Thruster Input Power, P, W	Thrust, F,N	Specific Impulse, I_{sp}, sec.	Thrust-to-Power, F/P, mN/kW	Overall Thruster Efficiency, η_t
50RC3, with 50 cm-diameter ion optics	1212	3.07	32.2	138	0.824	0.988	4256	0.171	3418	40.1	0.673
	1812	3.19	32.2	131	0.848	0.985	6314	0.216	4289	34.3	0.720
	1811	3.41	31.3	137	0.882	0.976	6761	0.229	4420	33.9	0.735
	1810	3.58	30.1	150	0.905	0.964	7138	0.238	4485	33.3	0.733
	2110	5.96	29.5	129	0.877	0.978	13,513	0.433	4750	32.0	0.746
50DIV, 50 cm-dia. Divergent-field	887	3.22	32.7	221	0.784	0.992	3682	0.154	2792	41.8	0.572
	1112	3.27	32.7	217	0.794	0.991	4461	0.175	3165	39.2	0.608
	1611	5.57	30.8	195	0.844	0.985	10,222	0.356	4024	34.9	0.688
	1340	6.03	35.5	200	0.889	0.974	9454	0.347	3821	36.8	0.689
	1516	6.13	35.5	196	0.897	0.970	10,665	0.374	4086	35.1	0.703
	1620	6.66	30.7	180	0.819	0.989	12,172	0.429	3931	35.2	0.679
	2021	6.86	31.0	176	0.838	0.986	15,258	0.492	4483	32.2	0.709
	1844	8.57	31.7	181	0.819	0.989	17,573	0.588	4194	33.5	0.689
	2118	8.84	31.7	174	0.839	0.986	20,490	0.649	4593	31.7	0.713
50RC1, with 30 cm-diameter ion optics	805	2.30	24.9	252	0.891	0.973	2527	0.103	2966	40.6	0.591
	1005	3.00	24.5	265	0.877	0.978	3920	0.150	3278	38.4	0.617
	1202	3.91	21.5	266	0.860	0.982	5864	0.215	3532	36.7	0.636
	1502	5.47	21.5	257	0.864	0.981	9779	0.336	3962	34.4	0.668
	1553	7.50	23.1	265	0.927	0.943	13,833	0.451	4154	32.6	0.664
50RC3, with 30 cm-diameter ion optics	1401	2.46	30.6	421	0.757	0.994	4580	0.148	3394	32.3	0.538
	1512	1.82	31.5	320	0.770	0.993	3419	0.114	3584	33.2	0.584

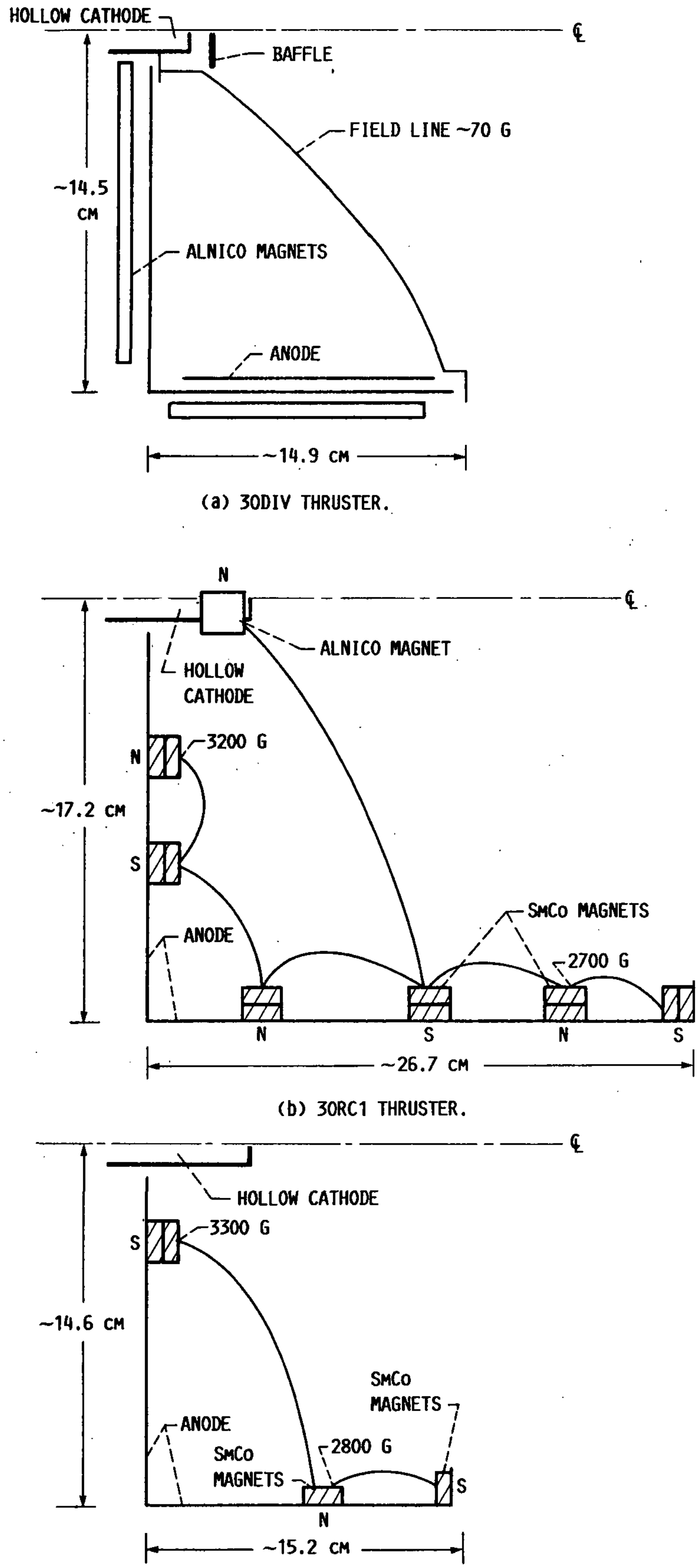

(a) 30DIV THRUSTER.

(b) 30RC1 THRUSTER.

(c) 30RC2 THRUSTER.

FIGURE 1. - CROSS-SECTION VIEW OF ION THRUSTERS, SHOWN APPROXIMATELY TO SCALE.

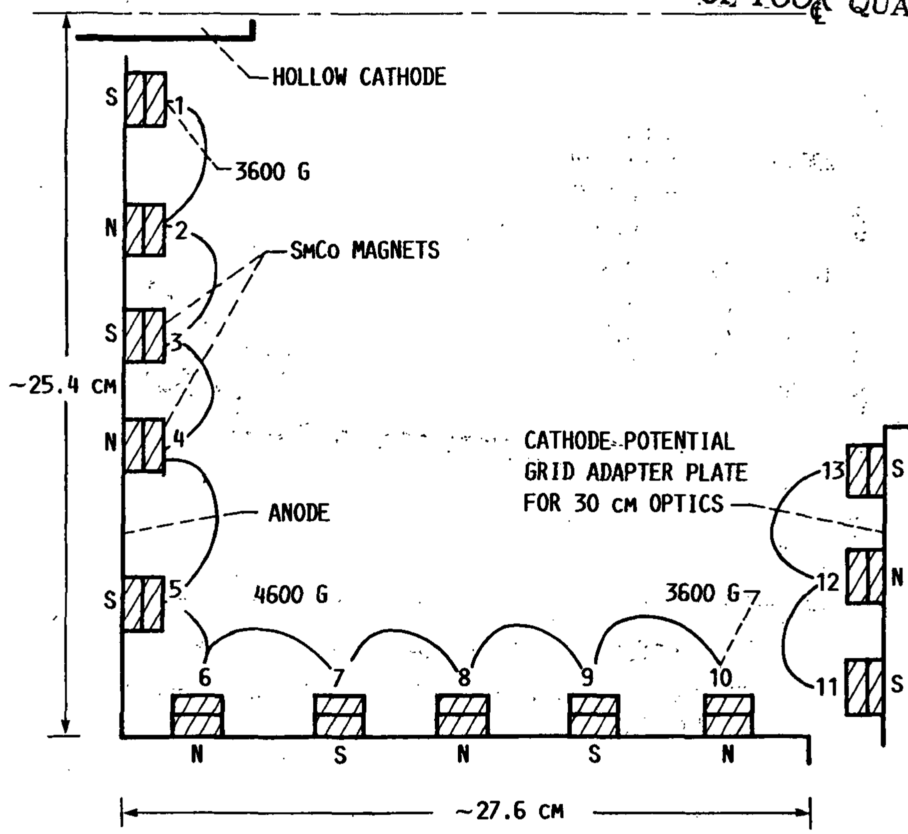

(d) 50RC1 THRUSTER.

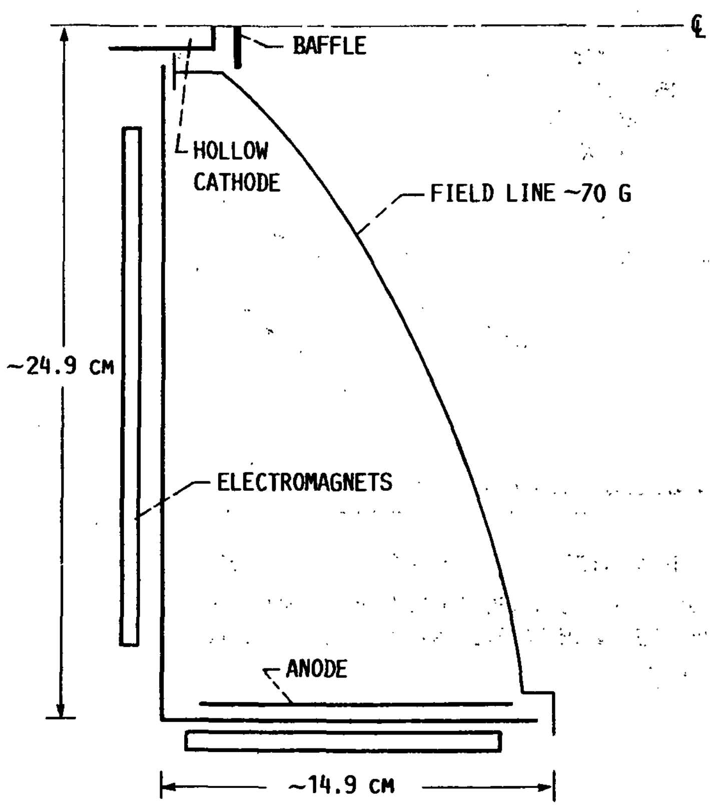

(e) 50DIV THRUSTER.

FIGURE 1. - CONCLUDED.

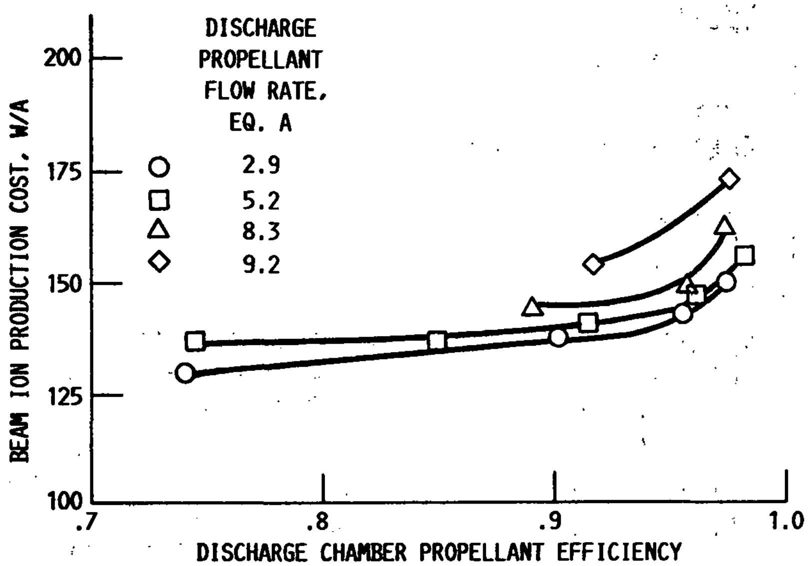

FIGURE 2. - DISCHARGE CHAMBER PERFORMANCE OF 30DIV THRUSTER.

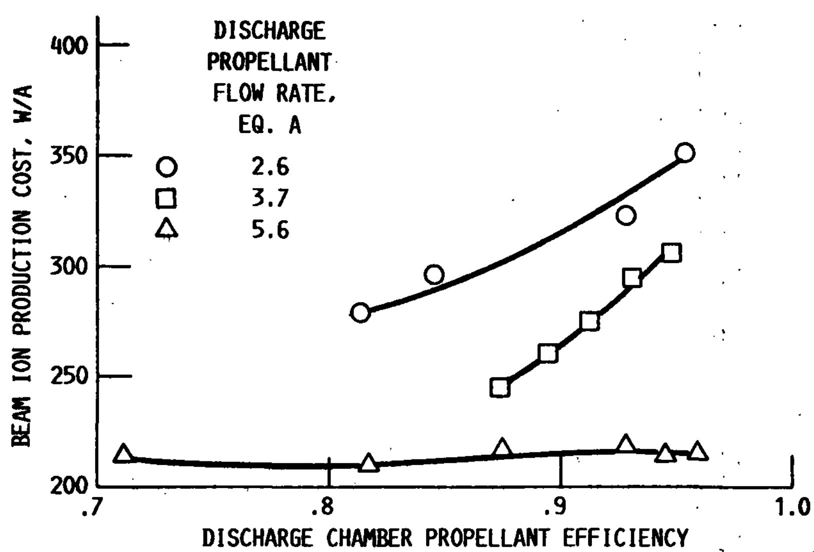

FIGURE 3. - DISCHARGE CHAMBER PERFORMANCE OF 30DIV THRUSTER WITH BAFFLE AND SUPPORT STRUCTURE REMOVED.

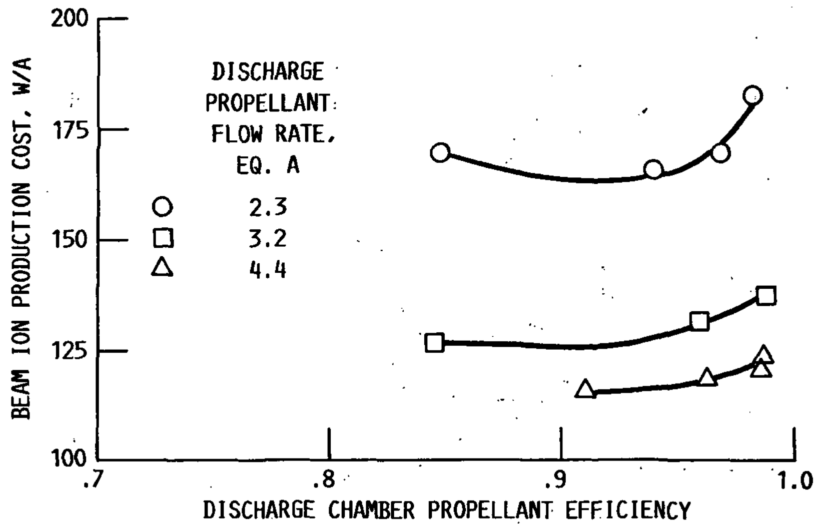

FIGURE 4. - DISCHARGE CHAMBER PERFORMANCE OF 30RC1 THRUSTER.

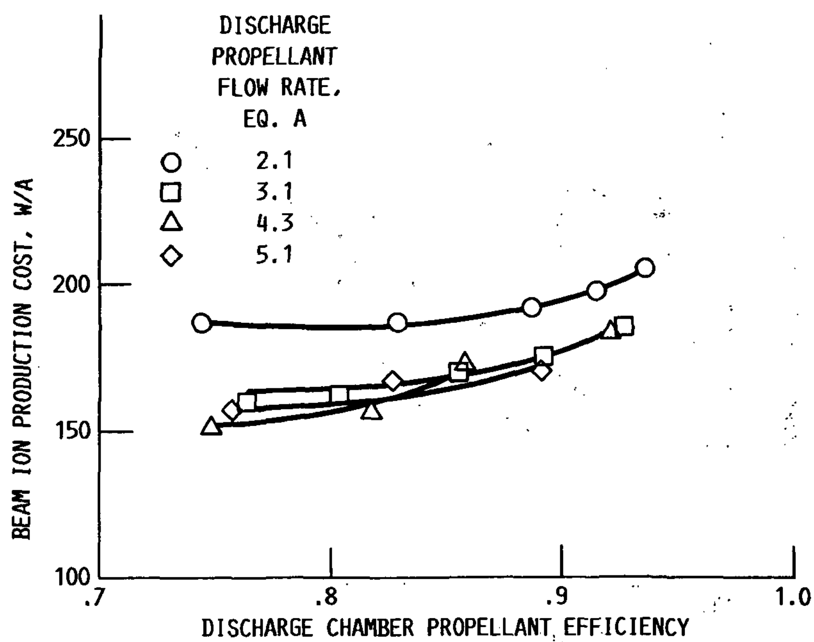

FIGURE 5. - DISCHARGE CHAMBER PERFORMANCE OF 30RC2 THRUSTER.

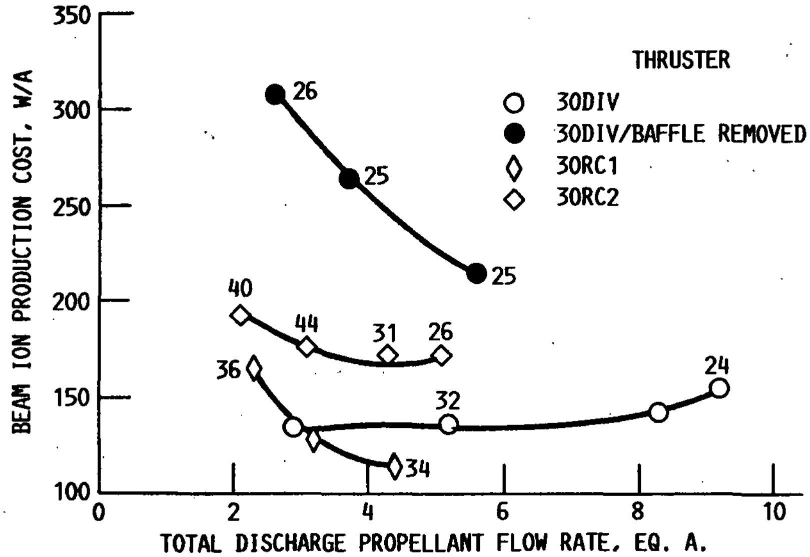

FIGURE 6. - THROTTLING COMPARISON AT NEAR 90% DISCHARGE CHAMBER PROPELLANT EFFICIENCY. DISCHARGE VOLTAGES ARE INDICATED.

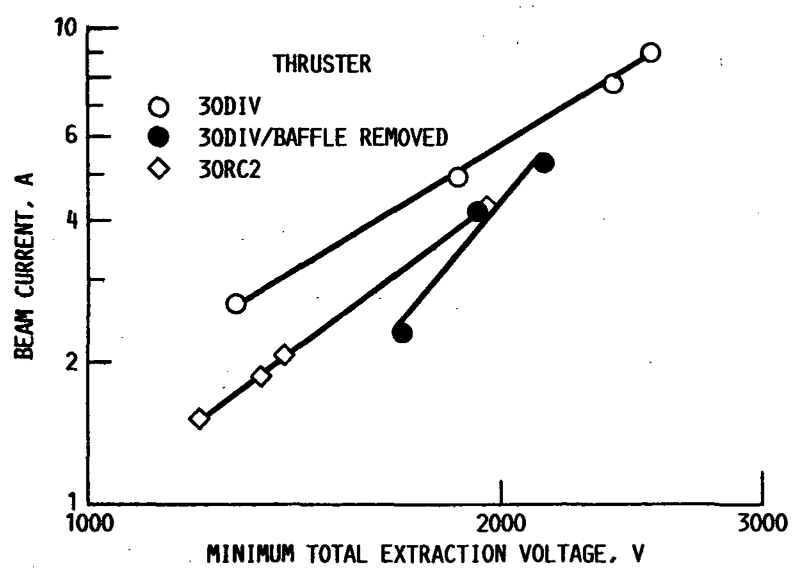

FIGURE 7. - PERFORMANCE OF 30-CM-DIAMETER ION OPTICS.

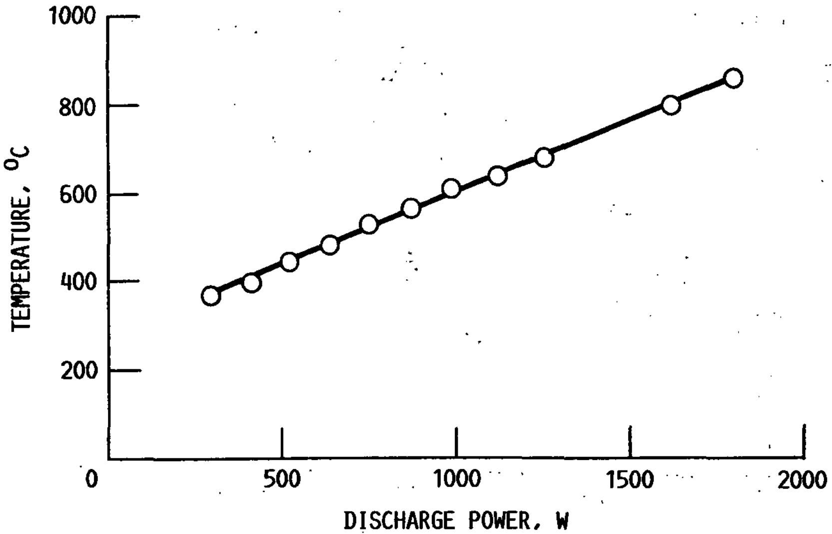

FIGURE 8. - MAXIMUM ION EXTRACTION SYSTEM TEMPERATURE AS A FUNCTION OF DISCHARGE POWR FOR THE 30DIV THRUSTER.

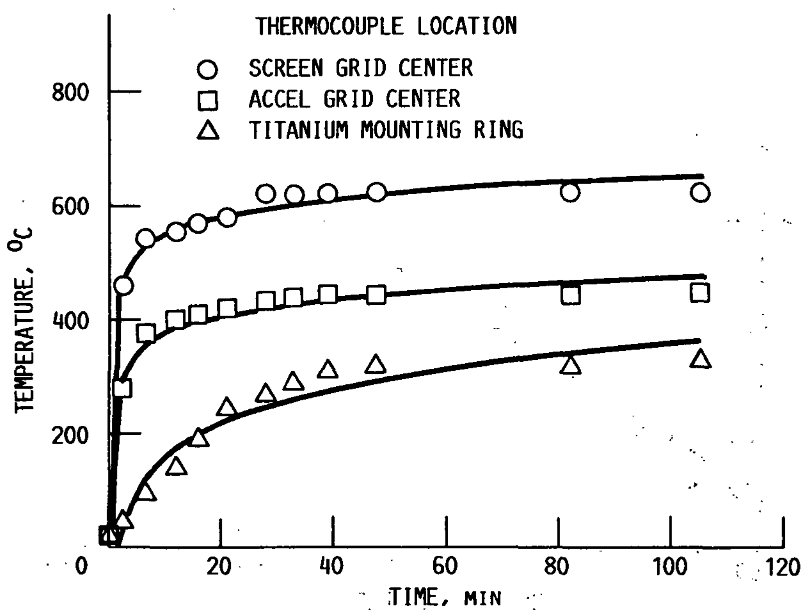

FIGURE 9. - ION EXTRACTION SYSTEM TEMPERATURE VERSUS TIME FROM DISCHARGE STARTUP AT 1200 W.

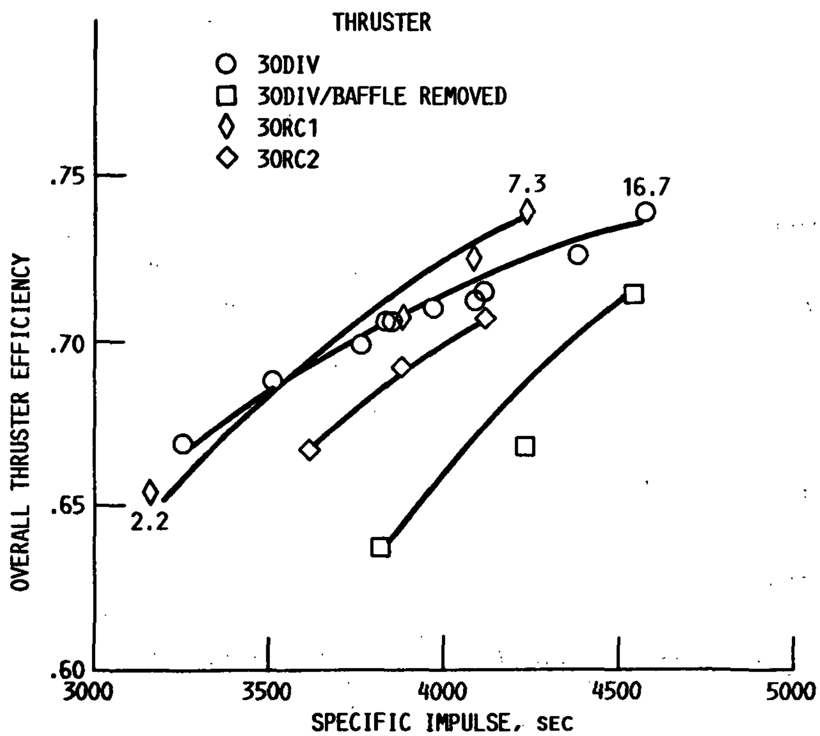

FIGURE 10. - THRUSTER PERFORMANCE COMPARISON AT NEAR 90% TOTAL PROPELLANT EFFICIENCY. THRUSTER INPUT POWER LEVELS, IN kW, ARE INDICATED.

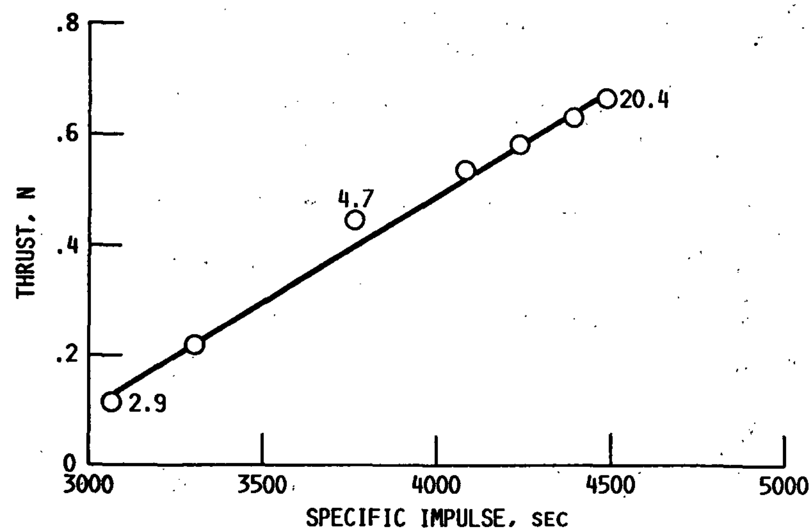

FIGURE 11. - THRUST VERSUS SPECIFIC IMPULSE FOR 30DIV THRUSTER. THRUSTER INPUT POWER LEVELS, IN kW, ARE INDICATED.

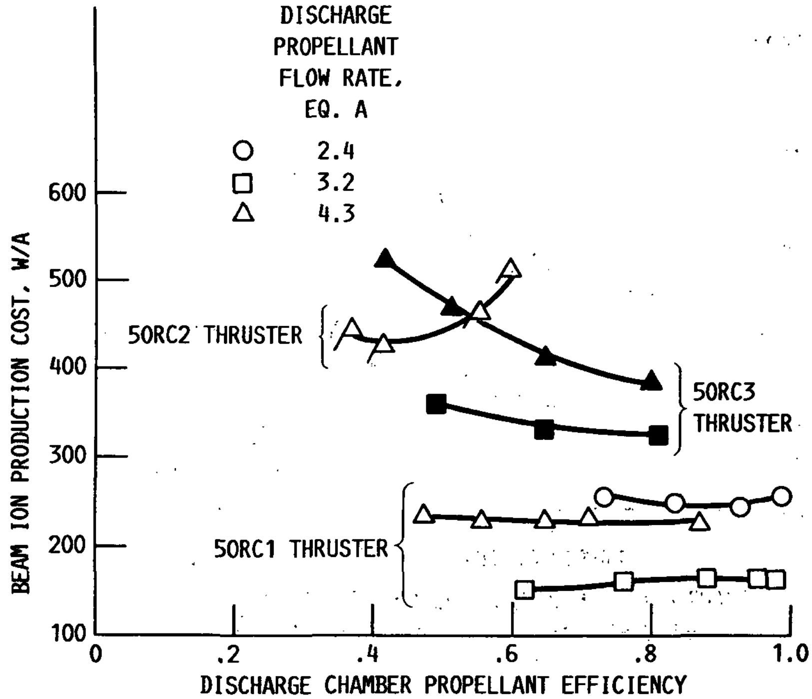

FIGURE 12. - DISCHARGE CHAMBER PERFORMANCE OF THREE 50-CM-DIAMETER RING-CUSP CONFIGURATIONS WITH 30-CM-DIAMETER ION OPTICS.

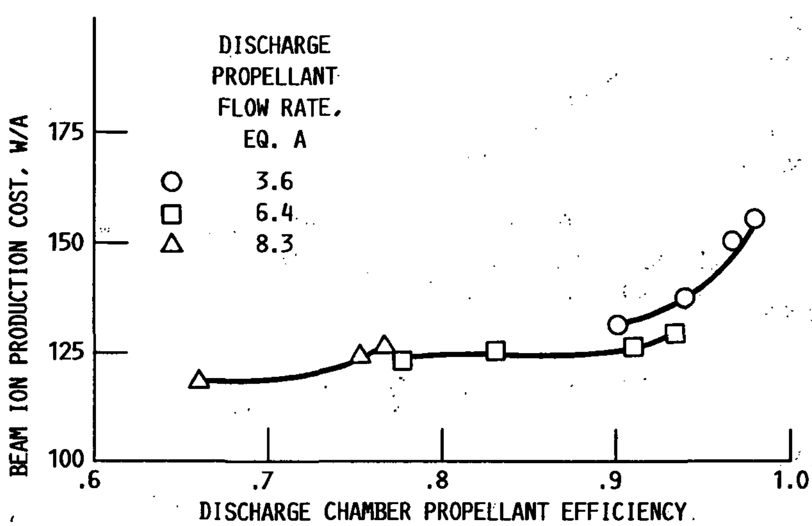

FIGURE 13. - DISCHARGE CHAMBER PERFORMANCE OF CONFIGURATION 50RC3 WITH 50-CM-DIAMETER ION OPTICS.

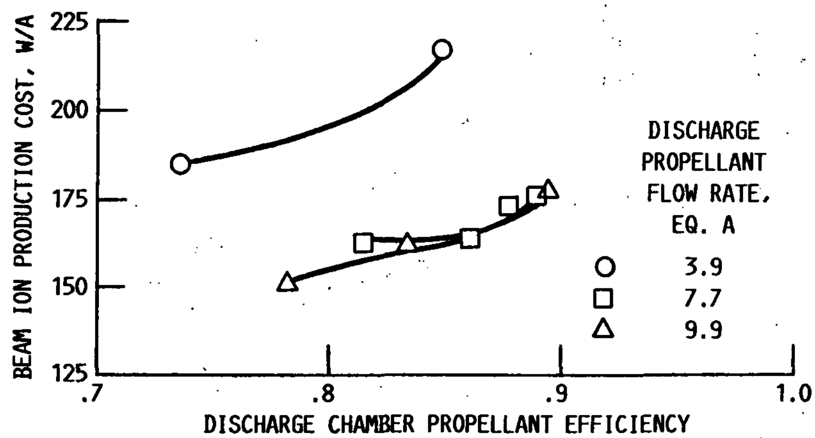

FIGURE 14. - DISCHARGE CHAMBER PERFORMANCE OF 50DIV THRUSTER, WITH 50-CM-DIAMETER ION OPTICS.

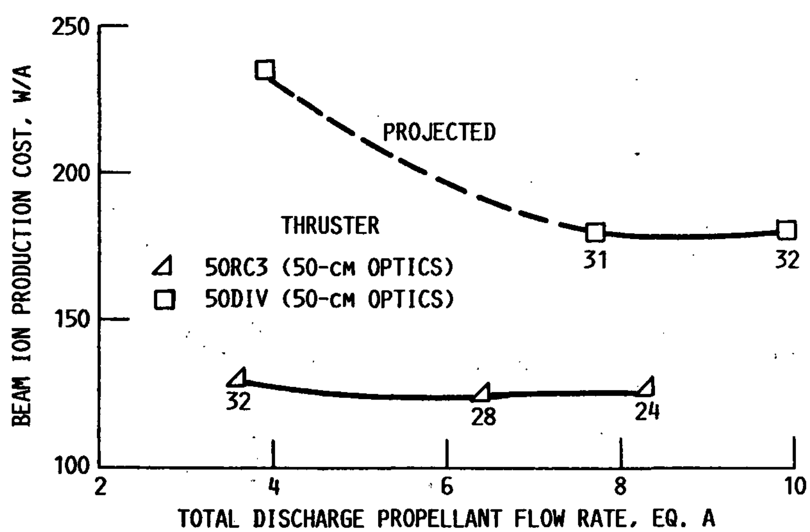

FIGURE 15. - THROTTLING COMPARISON AT NEAR 90% CHAMBER PROPELLANT EFFICIENCY. DISCHARGE VOLTAGES ARE INDICATED.

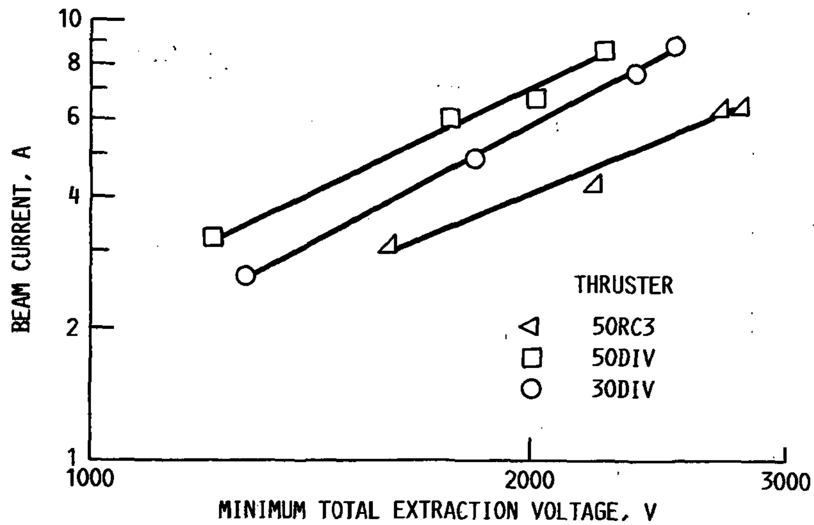

FIGURE 16. - PERFORMANCE OF 50-CM-DIAMETER ION OPTICS.

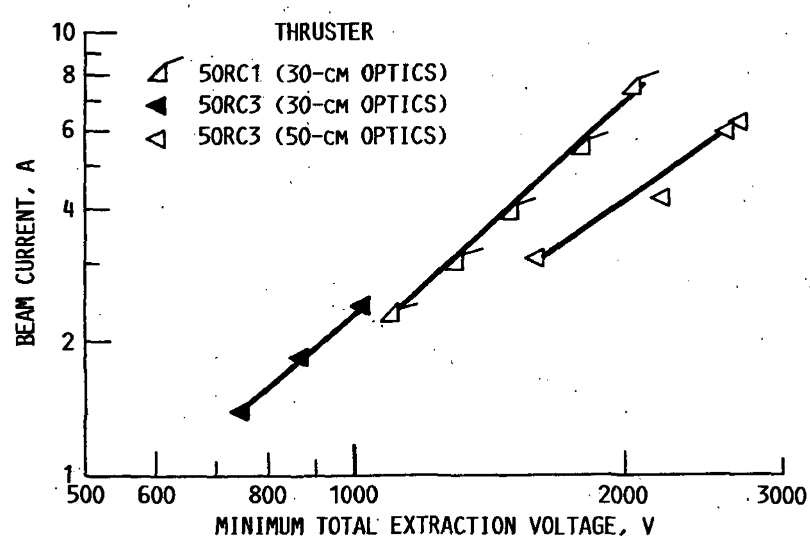

FIGURE 17. - COMPARISON OF 30-CM- AND 50-CM-DIAMETER ION OPTICS PERFORMANCE ON 50-CM RING-CUSP THRUSTER.

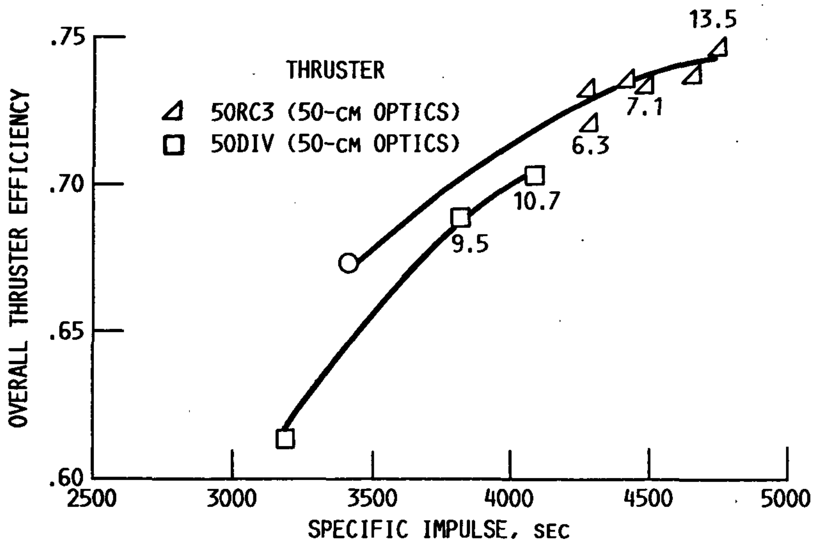

FIGURE 18. - THRUSTER PERFORMANCE COMPARISON AT NEAR 90% TOTAL PROPELLANT EFFICIENCY. THRUSTER INPUT POWER LEVELS, IN kW, ARE INDICATED.

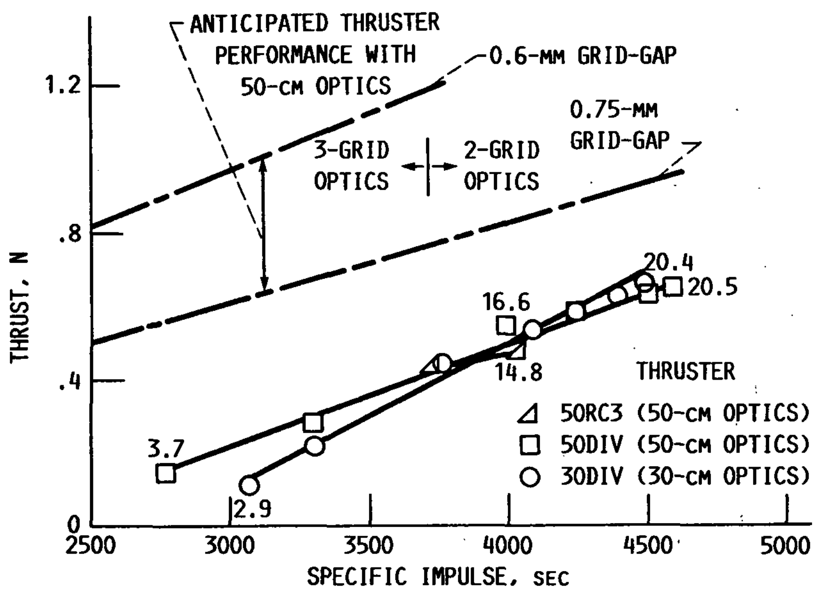

FIGURE 19. - THRUSTER PERFORMANCE COMPARISON. THRUSTER INPUT POWER LEVELS, IN kW, ARE INDICATED.

NASA
National Aeronautics and Space Administration

Report Documentation Page

1. Report No.	2. Government Accession No.	3. Recipient's Catalog No.
NASA TM-101292 AIAA-88-2914		

4. Title and Subtitle	5. Report Date
Performance of 10-kW Class Xenon Ion Thrusters	
	6. Performing Organization Code
7. Author(s) Michael J. Patterson and Vincent K. Rawlin	8. Performing Organization Report No. E-4272
	10. Work Unit No. 506-42-31
9. Performing Organization Name and Address National Aeronautics and Space Administration Lewis Research Center Cleveland, Ohio 44135-3191	11. Contract or Grant No.
	13. Type of Report and Period Covered Technical Memorandum
12. Sponsoring Agency Name and Address National Aeronautics and Space Administration Washington, D.C. 20546-0001	14. Sponsoring Agency Code

15. Supplementary Notes

Prepared for the 24th Joint Propulsion Conferences cosponsored by the AIAA, ASME, SAE, and ASEE, Boston, Masssachusetts, July 11-13, 1988.

16. Abstract

This paper presents performance data for laboratory and engineering model 30 cm-diameter ion thrusters operated with xenon propellant over a range of input power levels from approximately 2 to 20 kW. Also presented are preliminary performance results obtained from laboratory model 50 cm-diameter cusp- and divergent-field ion thrusters operating with both 30 cm- and 50 cm-diameter ion optics up to 20 kW input power. These data include values of discharge chamber propellant and power efficiencies, as well as values of specific impulse, thruster efficiency, thrust, and power. The operation of the 30 cm- and 50 cm-diameter ion optics are also discussed.

17. Key Words (Suggested by Author(s))	18. Distribution Statement
Xenon Ion thruster Primary space propulsion	Unclassified - Unlimited Subject Category 20

19. Security Classif. (of this report)	20. Security Classif. (of this page)	21. No of pages	22. Price*
Unclassified	Unclassified	30	A03

NASA FORM 1626 OCT 86

*For sale by the National Technical Information Service, Springfield, Virginia 22161

National Aeronautics and
Space Administration

Lewis Research Center
Cleveland, Ohio 44135

Official Business
Penalty for Private Use $300

FOURTH CLASS MAIL

ADDRESS CORRECTION REQUESTED

U.S.MAIL

Postage and Fees Paid
National Aeronautics and
Space Administration
NASA 451

NASA